Science Advances
AAAS

advances.sciencemag.org/cgi/content/full/4/11/eaat4556/DC1

Supplementary Materials for

Molecular fossils from phytoplankton reveal secular P_{CO_2} trend over the Phanerozoic

Caitlyn R. Witkowski*, Johan W. H. Weijers, Brian Blais, Stefan Schouten, Jaap S. Sinninghe Damsté

*Corresponding author. Email: caitlyn.witkowski@nioz.nl

Published 28 November 2018, *Sci. Adv.* **4**, eaat4556 (2018)
DOI: 10.1126/sciadv.aat4556

The PDF file includes:

Other Supplementary Material for this manuscript includes the following:

(available at advances.sciencemag.org/cgi/content/full/4/11/eaat4556/DC1)

Code S1 (.pdf format). Python code used for Monte Carlo simulations to calculate uncertainty for P_{CO_2} estimations by considering every parameter involved in the equations.
Data S1 (Microsoft Excel format). All data used to reconstruct P_{CO_2} from the $\delta^{13}C_{phytane}$.

Supplementary Materials and Methods

Marine oils were used to reconstruct periods where there was less sediment records available and make up 13% of our total data set. Marine oils were selected based on empirical, qualitative examination of the oil composition as tested by GC-MS. For example, strong indicators for marine conditions include the presence of C_{30} steranes and a lower pristane/phytane ratio (<1.5). In contrast, a high pristane/phytane ratio (>2) reflects terrestrial input. Strong indicators for terrestrial conditions include a higher C_{29} sterane content relative to other steranes, a higher C_{19} tricyclic content, a higher methylcyclohexane content, a low sulfur content, and sometimes odd-over-even n-alkane distribution (50). Other typical terrestrial biomarkers include oleanane, taraxastane, and bicadinanes, while tetracyclic polyprenoids indicate lacustrine environments.

Supplementary Text

Uncertainty analysis for calculating ε_p

As described in the main text, there are several calculations to derive pCO_2 estimations from the $\delta^{13}C$ of phytane. In order to constrain the uncertainty in our pCO_2 estimations, Monte Carlo simulations were run using the uncertainty associated with each individual equation parameter. The result of these simulations are probability distributions for each pCO_2 estimation given the input data and standard deviation on the input data. Here, we will describe the step-by-step equations needed for pCO_2 reconstruction and the impact of each individual equation parameter on the final outcome.

To calculate stable carbon isotopic fractionation associated with CO_2 fixation (ε_p), we use

$$\varepsilon_p = 1000 \cdot [(\delta_d+1000) / (\delta_p+1000) - 1] \quad (1)$$

where δ_p is the $\delta^{13}C$ of primary photosynthate and where δ_d is the $\delta^{13}C$ of aqueous carbon dioxide ($CO_{2(aq)}$) in the photic zone (*6, 7, 52*).

δ_p is estimated using:

$$\delta_p = \delta^{13}C \text{ of phytane} + \Delta\delta \quad (2)$$

where $\delta^{13}C$ of phytane is our raw data and $\Delta\delta$ represents the stable carbon isotopic offset between the biomarker phytane and biomass. $\delta^{13}C$ of phytane is assigned a standard deviation of ± 0.5 ‰ uniform distribution based on the maximum uncertainty associated with the IRMS instrumentation, although the error on measurements is general much lower (ca. ± 0.1 ‰) on samples run in triplicate. The $\delta^{13}C$ of phytane ± 0.5 ‰ uniform distribution may cause ca. 1.5% change in the final calculated ε_p.

To estimate the $\Delta\delta$ for phytane, laboratory culture experiments in which the $\delta^{13}C$ values for both algal biomass and phytol, the precursor of phytane, were compiled in Fig. S1 and Table S1 (references therein). Because the conversion of phytol to phytane does not involve the breaking of carbon bonds, there is likely a negligible difference in their isotopic composition due to diagenesis, unlike phytol's other diagenetic products such as pristane, which may be slightly depleted from the loss of a carbon atom (Schouten et al., 2008). Fig. S1 shows the average $\Delta\delta$ with standard deviation for each species, as well as the overall average for the dataset of 3.5‰ shown by the thin gray line with one standard deviation shaded in light gray (± 1.3‰ standard

deviation) and two in dark gray. The data for *Alexandrium tamarense* was not included as it is a significant outlier ($P < 0.05$) using the Grubb's outlier test, with a Z value of 2.84 where the critical value is 2.78. The $\Delta\delta$ for phytane ± 1.3 ‰ standard deviation may cause ca. 3.5% change in ε_p. In other words, the uncertainty in this parameter may cause the final calculated ε_p to vary by ± 0.7 ‰. All data and references can be found in Table S1.

To estimate δ_d, the $\delta^{13}C$ of aqueous carbon dioxide ($CO_{2(aq)}$) in the photic zone, we use the $\delta^{13}C$ of planktonic foraminifera:

$$\delta_d = \delta^{13}C \text{ of planktonic foraminifera} - 1 + \varepsilon_{b(a)} \quad (3)$$

where $\delta^{13}C$ of carbonate of planktonic foraminifera (see references within Dataset S1) and subtraction of 1 refers to the nearly constant $\delta^{13}C$ difference in calcite ($CaCO_3$) from bicarbonate (HCO_3^-) due to abiotic kinetic fractionation, which consequently effects the $\delta^{13}C$ between foraminiferal calcite relative to DIC (*53*). $\varepsilon_{b(a)}$ describes the carbon isotopic fractionation of $CO_{2(aq)}$ with respect to HCO_3^-.

The $\delta^{13}C$ of carbonate of planktonic foraminifera was preferentially used from the same site as phytane; in the cases where this data was not available, data from nearby sites were used; where that was not available, the long term global average of $\delta^{13}C$ of marine carbonate as calculated by Hayes *et al.* (*8*) was used. The instrumental error for $\delta^{13}C$ of carbonate is ± 0.2 ‰ uniform distribution, although the error on measurements is generally much lower (ca. ± 0.01 ‰) based on samples run in triplicate. However, because some estimates are obtained from the global average (*8*), we expand this standard deviation by twofold to ± 0.4 ‰ uniform distribution. The $\delta^{13}C$ of planktonic foraminifera ± 0.4 ‰ uniform distribution may cause ca. 0.5 % change in ε_p, resulting ± 0.2 ‰ change to the final calculated ε_p.

$\varepsilon_{b(a)}$ describes the carbon isotopic fractionation of $CO_{2(aq)}$ with respect to HCO_3^-, which depends on temperature, and which can be calculated using the equation:

$$\varepsilon_{b(a)} = 24.12 - 9866/\,T \quad (4)$$

where T is temperature in Kelvin (*16*). Temperatures were estimated from sea surface temperature proxies reported for the same site. Where SST data for the site is unavailable, temperature was estimated by adjusting the modern site for its paleolatitude (using www.paleolatitude.org), finding the SST at that location (e.g. seatemperature.org), and then correcting the present-day SST for global temporal SST anomalies e.g. (*30, 31*) for 0-56 Ma; (*32*) for 65-455 Ma. References for temperature estimations are included in Dataset S1. SST is ± 4ºC standard deviation in our uncertainty calculations. Although SST proxies generally have a lower uncertainty than 4ºC, we expanded this uncertainty due to the occasional lack of local data and due to the large timespan, i.e. uncertainties in temperature estimates substantially increase with deep time due to a lack of accurate proxies. The uncertainty of ± 4ºC standard deviation may cause ca. 1.2 % change in ε_p, equivalent to the final calculated ε_p ± 0.2 ‰.

Uncertainty analysis for estimating pCO_2

To estimate the dissolved carbon dioxide ($CO_{2[aq]}$) from ε_p we use

$$CO_{2[aq]} = b / (\varepsilon_f - \varepsilon_p) \quad (5)$$

a relationship developed by Hayes (*17*) and Francois *et al.* (*39*) and which is a modification of

the relationship developed for higher plants from Farquhar *et al.* (*4*, *40*).

The term *b* accounts for all factors that may influence isotopic fractionation in addition to carbon dioxide, equivalent to environmental (C_e) versus intracellular (C_i) concentrations of $CO_{2[aq]}$ as related to isotopic fractionation due to CO_2-fixation (ε_f) versus due to diffusive transport (ε_t), expressed as (C_e–C_i) (ε_f –ε_t) (*54*). Cell carbon allocation and bicarbonate uptake, as well as growth rate and cell geometry, influence carbon acquisition into the cell e.g. (*9*) and therefore the term *b*. Because this is the first study to apply phytane towards secular trends in pCO_2, there have not yet been laboratory cultures and environmental samples to constrain phytane in regards to *b*. Modern environmental samples suggest a correlation of *b* values for alkenones with phosphate concentrations where $b = (118.52\ [PO_4^{3-}]) + 84.07$ when ε_f is 25‰ (*35*, *41*, *42*, *55*). Thus, within normal environmental ranges for PO_4^{3-} (~0-2 µM), *b* for alkenone-producers ranges from approximately 70-240 ‰ kg μM^{-1} with a mean of 165 ± 53 standard deviation. Because phytane is coming from the entire phytoplankton community, we also calculated *b* from the $\delta^{13}C$ of total organic matter in diverse modern open marine sediments (Table S2), which yielded an average *b* of 168 ± 43 ‰ kg μM^{-1} standard deviation. Marine organic matter, just like phytol/phytane, is also predominantly derived from diverse phytoplanktonic sources, although it likely contains contributions from non-photosynthetic algae, bacteria and archaea, in addition to smaller amounts of continental organic matter. Nevertheless, the average *b* of 168 ‰ kg μM^{-1} is identical to that calculated using alkenones, indicating that this estimation of *b* can also be applied to a common phytoplanktonic biomarker. Hence, for our calculations, a mean value of 170 ‰ kg μM^{-1} is used for *b*, consistent with the *b* used in previous phytane-based pCO_2 estimations (*22*, *23*). In further consideration of increased uncertainty over the geologic record, we conservatively expand the ± 43 ‰ kg μM^{-1} standard deviation up to ± 60 ‰ kg μM^{-1} standard deviation. This range is further supported by Bidigare et al. (*42*) where the $\delta^{13}C$ of phytol was measured the equatorial Pacific Ocean (from 3°N to 2°S, 140°W). In Table S3, we calculate *b* from the reported $\delta^{13}C$ of phytol suspended particulate matter (and hence derived from a variety of phytoplankton species), which shows minor variability over the 500 km transect. The average *b* for this very low-productivity region (b = 107±5) is indeed at the low end of our window for *b* (170±60). We assume *b* is a constant over time as we have no means of constraining how *b* can vary with time. The uncertainty analysis shows that changes in *b* shifts absolute estimates of pCO_2 but not the overall trend. Our uncertainty analysis shows that a 1% change in *b* yields a 1% change in pCO_2 (Fig. S3A).

ε_f is the maximum isotopic fractionation associated with photosynthetic carbon fixation, generally ranging from 25–28‰ for algae in modern oceans and laboratory experiments (*43*, *44*). Because phytane is the average of the entire phytoplankton community, it is not possible to know the exact percentage of species contributions to the phytane pool. Thus, a constant average fractionation from laboratory cultures of 26.5‰ was used for the entire dataset. Our observed ε_p which does not surpass 25‰ suggests that there have not been dramatic changes in the isotopic fractionation due to evolutionary changes in Rubisco, which may occur due to environmental stressors e.g. low environmental carbon (*38*). Because we are using the averaged maximum fractionation from all phytoplankton species and because our data suggests there were no major evolutionary changes in this fractionation, ε_f is likely relatively constant. Using the full range of 25–28‰, we explore ± 1.5‰ uniform distribution uncertainty on the effect of ε_f on the resulting pCO_2 estimation. In Fig. S3, ε_f has a varying influence on pCO_2 estimations, averaging around a ±10% change in pCO_2 estimation for periods of lower pCO_2 to averaging around -15/+30% for most of the Phanerozoic. There is a positive bias, where there is much more uncertainty in the

positive direction (maximum 80%) than in the negative (maximum -30%). This positive bias is caused when ε_f and ε_p approach one another, as seen during the Paleocene/Eocene transition (Fig. S3B).

To estimate the atmospheric concentration of carbon dioxide from the $CO_{2[aq]}$ we use:

$$pCO_2 = [CO_{2(aq)}] / K_0 \quad (6)$$

based on Henry's Law, where the solubility constant K_0, expressed in M/atm, is:

$$\ln K_0 = A_1 + A_2(100/T) + A_3 \ln(T/100) + S‰ [B_1 + B_2(T/100) + B_3(T/100)^2] \quad (7)$$

where A and B are constants, T is the temperature in Kelvin, and S‰ is salinity in ‰ (*56*)(Weiss, 1974). The constants used here are A_{1-3} (-58.0931, 90.5069, 22.2940) and B_{1-3} (0.02777,-0.02589, 0.00506), respectively (*45*). Because paleosalinity proxies are very limited, we here set a constant salinity of 34 ‰ ± 2 ‰ standard deviation. We include a second SST uncertainty of ± 4°C standard deviation (in addition to the ε_p estimations) in our estimations for pCO_2. For cooler periods, such as the Miocene towards today, this ± 4°C standard deviation results in a 10% potential influence on reconstructed pCO_2. For extremely warm periods, there is greater uncertainty; on average, uncertainty is ca. 20% with the highest uncertainty of 40% shown in the case of the Paleocene/Eocene transition.

All data used for these calculations are in Dataset S1 (*8, 22, 23, 25, 29-32, 57-95*).

Impact of O_2 on isotopic fractionation

Because Rubisco has the dual carboxylase-oxygenase function, some studies have speculated that the ratio of O_2 to CO_2 concentrations in the atmosphere may have an influence on a isotopic discrimination, e.g. (*96*). This may be a potential caveat for reconstructing pCO_2 during periods within earth history with substantially elevated atmospheric O_2 concentrations. However, it should also be noted that Berner et al. (*96*) based this discussion on four data points from a single species of diatom (though diatoms never experienced extremely high oxygen concentrations in their evolutionary history). Furthermore, the diatom was cultured under two simultaneously varying parameters, O_2 and CO_2. After the proposed model in the paper (*96*) had been applied to the data, there is only a $\leq$ 1‰ shift in the resulting fractionation. Such an effect is relatively minor compared to other assumptions in the overall approach (e.g., estimation of *b*). Furthermore, our record only contains a few data points from the period of presumed elevated atmospheric O_2 concentrations (ca. 240-350 Ma) and there is no apparent match between ε_p and periods of elevated O_2 concentrations.

(Ref 32, 51-96)

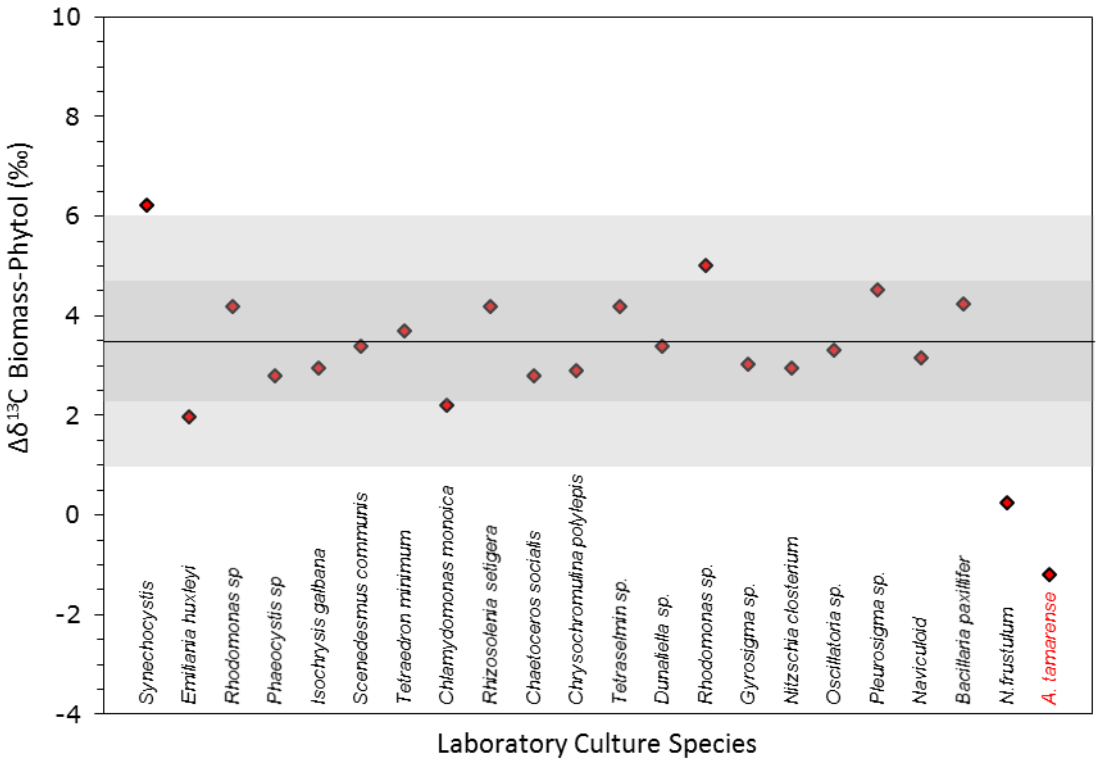

Fig. S1. Isotopic offset between biomass and phytol. On the x-axis are laboratory culture experiments from individual species of phytoplankton. The black line represents the mean, the dark band is the first standard deviation, and the light band is the second standard deviation for the entire set of phytoplankton. All references can be found in Table S1.

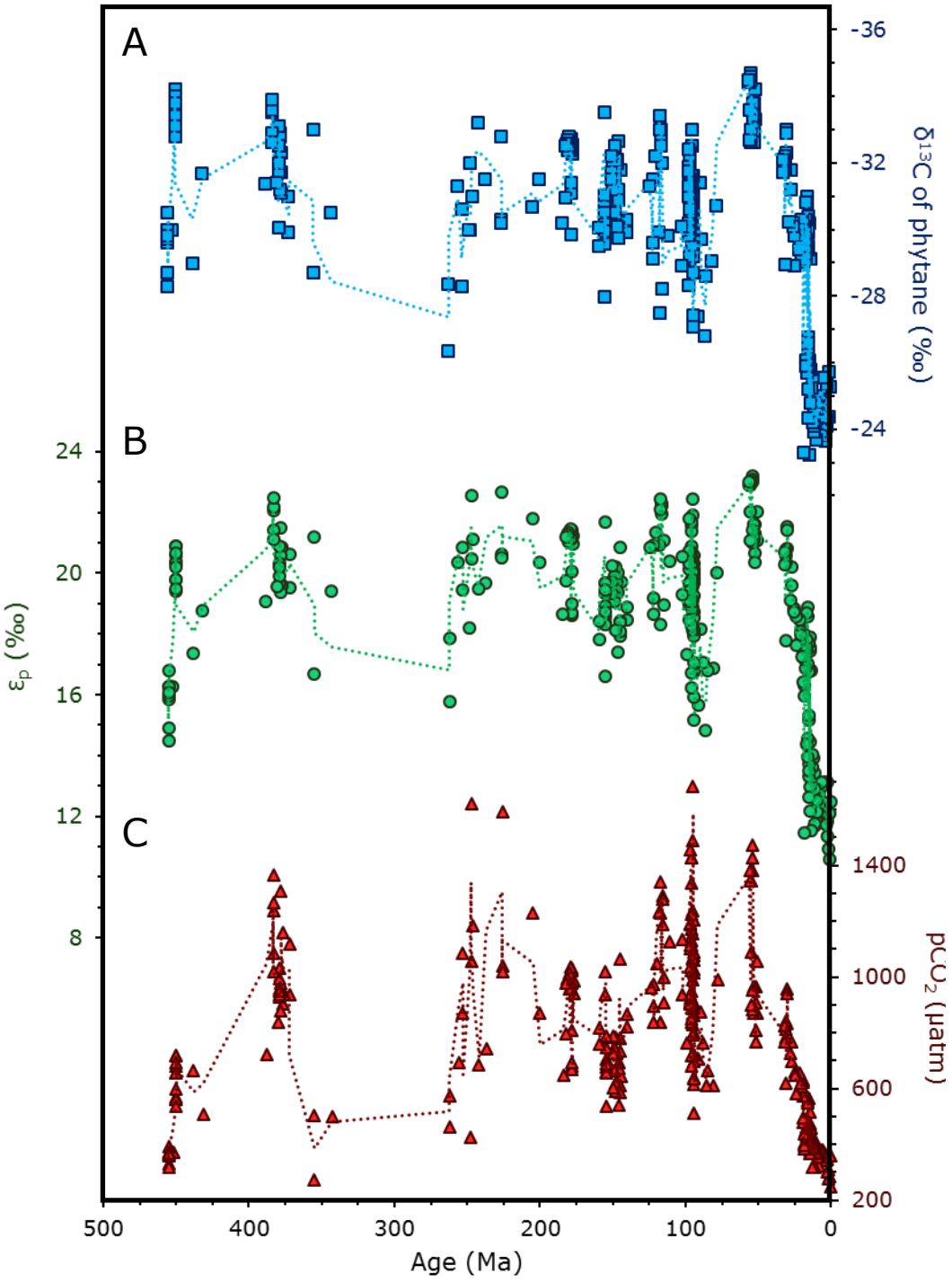

Fig. S2. Trends from reported $\delta^{13}C_{phytane}$ data to PCO_2. Phytane data over the Phanerozoic for A) $\delta^{13}C$, B) calculated ε_p, and C) estimated pCO_2.

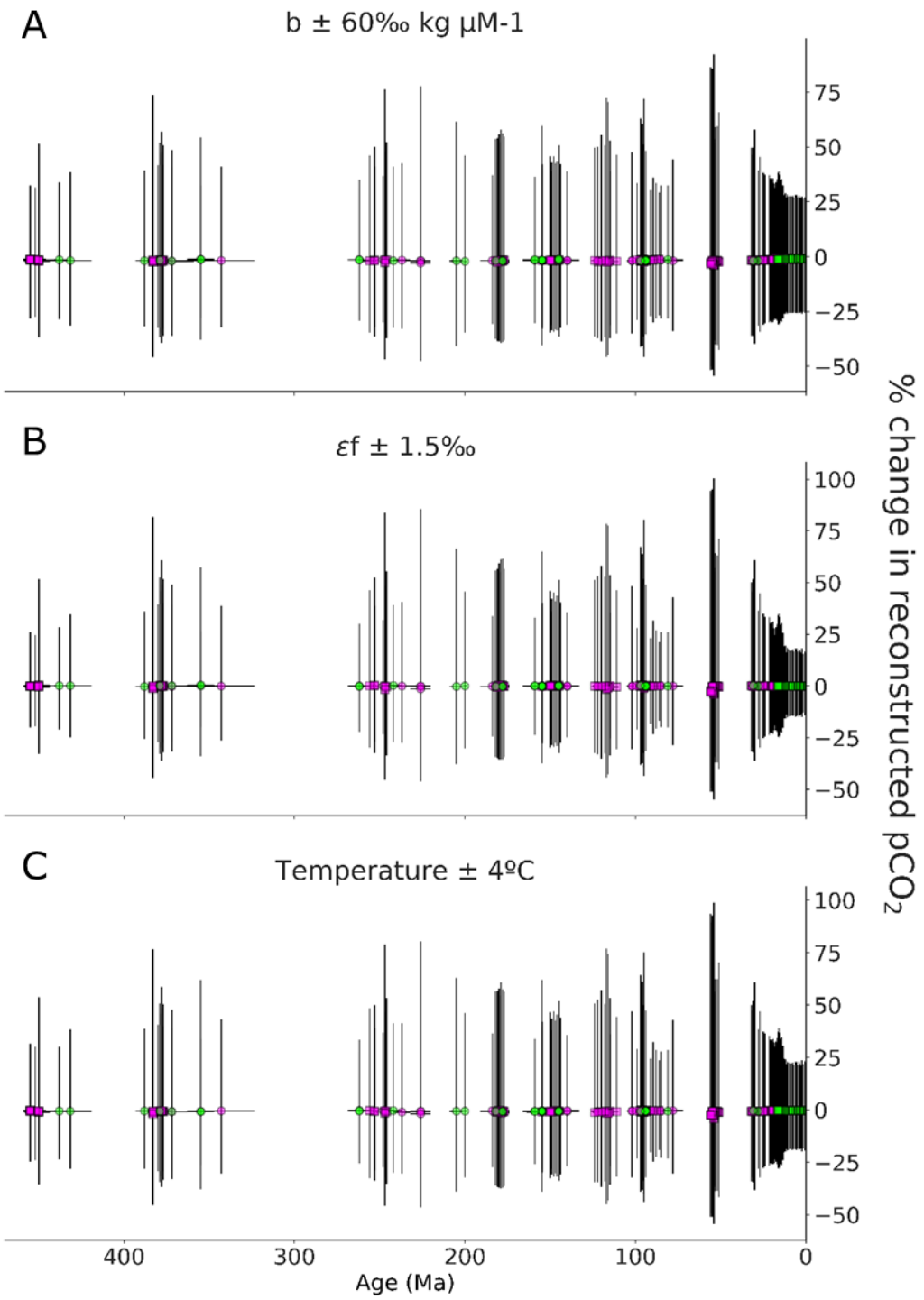

Fig. S3. Uncertainties associated with equation parameters. Percentage change in reconstructed pCO_2 given the following uncertainties within each equation parameter, A) b ± 60 ‰ kg μM^{-1} standard deviation, B) ε_f ± 1.5 ‰ uniform distribution, and C) temperature ± 4°C standard deviation.

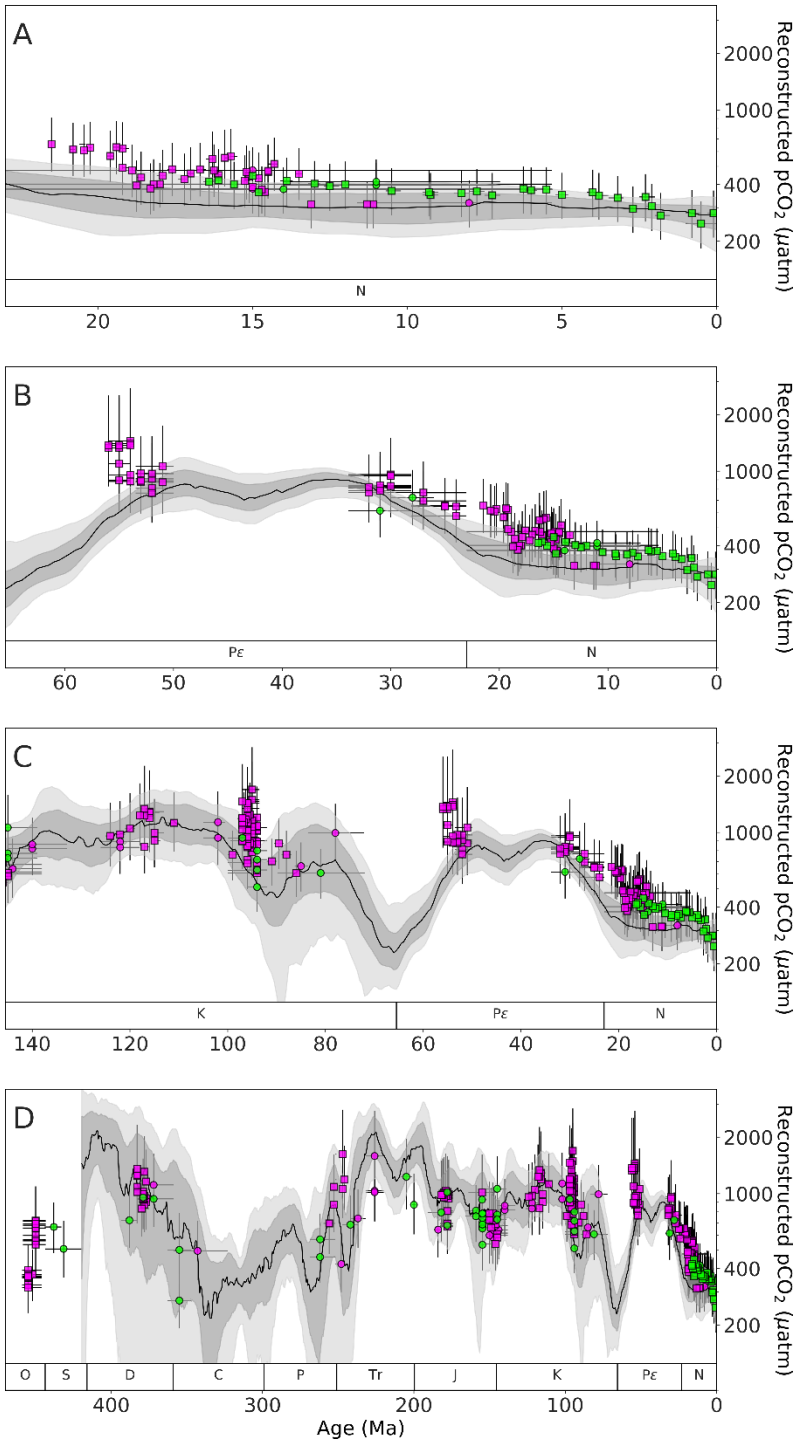

Fig. S4. *P*CO2 from phytane over the Phanerozoic in time slices.

Estimated pCO_2 (on a log-scale) from literature (pink) and new data (blue), by sediment (square) and oil (circle). Horizontal error bars indicate age uncertainty. Vertical error bars indicate uncertainty in estimation. Foster et al. compilation of pCO_2 proxies with LOESS fit (line) with 68 and 95% confidence intervals in gray and light gray plotted for comparison. A) Neogene, B) Paleogene, C) Cretaceous, and D) Phanerozoic.

Table S1. Isotopic offset between biomass and phytol. $\delta^{13}C$ of bulk biomass and phytol for each individual laboratory cultured species; $\Delta = \delta^{13}C$ offset between biomass and phytol; Genus refers to the cultured phytoplankton. The averages of each species are shown in Fig. S1.

$\delta^{13}C$ Biomass	$\delta^{13}C$ Phytol	Δ	Genus	Reference
-30.6	-36.5	5.9	*Synechocystis*	Sakata et al., 1997
-31.5	-38.4	7.0	*Synechocystis*	Sakata et al., 1997
-31.2	-37.0	5.8	*Synechocystis*	Sakata et al., 1997
-16.9	-18.2	1.3	*Emiliania huxleyi*	Riebesell et al., 2000
-17.3	-19.4	2.1	*Emiliania huxleyi*	Riebesell et al., 2000
-17.7	-20.3	2.6	*Emiliania huxleyi*	Riebesell et al., 2000
-17.7	-20.2	2.5	*Emiliania huxleyi*	Riebesell et al., 2000
-19.1	-21.1	2.0	*Emiliania huxleyi*	Riebesell et al., 2000
-21.2	-23.1	1.9	*Emiliania huxleyi*	Riebesell et al., 2000
-21.4	-23.3	1.9	*Emiliania huxleyi*	Riebesell et al., 2000
-22.0	-23.7	1.7	*Emiliania huxleyi*	Riebesell et al., 2000
-24.4	-25.9	1.5	*Emiliania huxleyi*	Riebesell et al., 2000
-26.6	-28.9	2.3	*Emiliania huxleyi*	Riebesell et al., 2000
-12.1	-16.3	4.2	*Rhodomonas sp.*	van Dongen et al., 2002
-17.5	-20.3	2.8	*Phaeocystis sp.*	van Dongen et al., 2002
-25.6	-31.2	5.6	*Spaghnum cuspidatum*	van Dongen et al., 2002
-13.8	-14.8	1.0	*Isochrysis galbana*	van Dongen et al., 2002
-15.7	-20.6	4.9	*Isochrysis galbana*	Schouten et al., 1998
-41.0	-44.4	3.4	*Scenedesmus communis*	Schouten et al., 1998
-49.5	-52.3	2.8	*Tetraedron minimum (batch)*	Schouten et al., 1998
-32.6	-37.2	4.6	*Tetraedron minimum (cont)*	Schouten et al., 1998
-43.9	-46.1	2.2	*Chlamydomonas monoica*	Schouten et al., 1998
-18.1	-22.3	4.2	*Rhizosolenia setigera*	Schouten et al., 1998
-17.7	-20.5	2.8	*Chaetoceros socialis*	Schouten et al., 1998
-14.2	-17.1	2.9	*Chrysochromulina polylepis*	Schouten et al., 1998
-16.9	-21.1	4.2	*Tetraselmin sp.*	Schouten et al., 1998
-22.8	-26.2	3.4	*Dunaliella sp.*	Schouten et al., 1998
-15.4	-20.4	5.0	*Rhodomonas sp.*	Schouten et al., 1998
-19.8	-23.0	3.2	*Gyrosigma sp.*	Oakes et al., 2005
-21.4	-25.9	4.5	*Gyrosigma sp.*	Oakes et al., 2005
-21.5	-23.6	2.1	*Gyrosigma sp.*	Oakes et al., 2005
-20.2	-24.6	4.4	*Gyrosigma sp.*	Oakes et al., 2005
-23.9	-26.8	2.9	*Gyrosigma sp.*	Oakes et al., 2005
-19.4	-23.7	4.3	*Gyrosigma sp.*	Oakes et al., 2005
-22.1	-31.1	9.0	*Gyrosigma sp.*	Oakes et al., 2005
-22.0	-25.3	3.3	*Gyrosigma sp.*	Oakes et al., 2005
-22.8	-28.7	5.9	*Gyrosigma sp.*	Oakes et al., 2005
-22.1	-22.6	0.5	*Gyrosigma sp.*	Oakes et al., 2005
-27.2	-27.8	0.7	*Gyrosigma sp.*	Oakes et al., 2005
-27.6	-26.3	-1.3	*Gyrosigma sp.*	Oakes et al., 2005
-23.7	-25.1	1.4	*Gyrosigma sp.*	Oakes et al., 2005
-23.5	-24.6	1.1	*Gyrosigma sp.*	Oakes et al., 2005
-22.4	-26.0	3.6	*Gyrosigma sp.*	Oakes et al., 2005

-19.6	-27.2	7.6	*Nitzschia closterium*	Oakes et al., 2005
-16.4	-19.3	2.9	*Nitzschia closterium*	Oakes et al., 2005
-20.1	-27.0	6.9	*Nitzschia closterium*	Oakes et al., 2005
-16.4	-19.4	3.0	*Nitzschia closterium*	Oakes et al., 2005
-20.3	-27.8	7.5	*Nitzschia closterium*	Oakes et al., 2005
-16.3	-20.5	4.2	*Nitzschia closterium*	Oakes et al., 2005
-16.0	-19.6	3.6	*Nitzschia closterium*	Oakes et al., 2005
-28.7	-34.2	5.5	*Nitzschia closterium*	Oakes et al., 2005
-21.9	-23.9	2.0	*Nitzschia closterium*	Oakes et al., 2005
-20.6	-22.2	1.6	*Nitzschia closterium*	Oakes et al., 2005
-16.2	-19.3	3.1	*Nitzschia closterium*	Oakes et al., 2005
-16.1	-19.2	3.1	*Nitzschia closterium*	Oakes et al., 2005
-17.0	-20.5	3.5	*Nitzschia closterium*	Oakes et al., 2005
-17.1	-22.6	5.5	*Nitzschia closterium*	Oakes et al., 2005
-31.8	-36.4	4.6	*Nitzschia closterium*	Oakes et al., 2005
-20.0	-18.3	-1.7	*Nitzschia closterium*	Oakes et al., 2005
-20.2	-18.7	-1.5	*Nitzschia closterium*	Oakes et al., 2005
-19.1	-17.4	-1.7	*Nitzschia closterium*	Oakes et al., 2005
-21.2	-18.7	-2.5	*Nitzschia closterium*	Oakes et al., 2005
-17.2	-19.1	1.8	*Nitzschia closterium*	Oakes et al., 2005
-23.1	-29.1	6.0	*Oscillatoria sp.*	Oakes et al., 2005
-25.9	-26.5	0.6	*Oscillatoria sp.*	Oakes et al., 2005
-26.8	-33.0	6.2	*Pleurosigma sp.*	Oakes et al., 2005
-27.8	-31.7	3.8	*Pleurosigma sp.*	Oakes et al., 2005
-20.3	-23.9	3.6	*Pleurosigma sp.*	Oakes et al., 2005
-24.6	-22.9	-1.6	*Naviculoid sp. 2*	Oakes et al., 2005
-22.6	-25.2	2.7	*Naviculoid sp. 2*	Oakes et al., 2005
-25.9	-26.8	0.9	*Naviculoid sp. 2*	Oakes et al., 2005
-23.4	-21.9	-1.5	*Naviculoid sp. 2*	Oakes et al., 2005
-23.1	-23.5	0.5	*Naviculoid sp. 2*	Oakes et al., 2005
-22.2	-28.9	6.7	*Naviculoid sp. 2*	Oakes et al., 2005
-24.7	-27.2	2.5	*Naviculoid sp. 1*	Oakes et al., 2005
-23.8	-30.0	6.1	*Naviculoid sp. 1*	Oakes et al., 2005
-25.5	-30.3	4.8	*Naviculoid sp. 1*	Oakes et al., 2005
-22.4	-28.8	6.4	*Naviculoid sp. 1*	Oakes et al., 2005
-25.9	-33.3	7.3	*Naviculoid sp. 1*	Oakes et al., 2005
-25.3	-28.0	2.7	*Bacillaria paxillifer*	Oakes et al., 2005
-21.6	-27.4	5.8	*Bacillaria paxillifer*	Oakes et al., 2005
-18.2	-18.6	0.4	*Nitzschia frustulum*	Oakes et al., 2005
-18.1	-19.0	0.9	*Nitzschia frustulum*	Oakes et al., 2005
-16.6	-17.5	0.9	*Nitzschia frustulum*	Oakes et al., 2005
-15.2	-15.5	0.3	*Nitzschia frustulum*	Oakes et al., 2005
-16.6	-15.3	-1.3	*Nitzschia frustulum*	Oakes et al., 2005
-59.3	-61.0	1.7	*Alexandrium tamarense*	Wilkes et al., 2017
-54.5	-52.0	-2.5	*Alexandrium tamarense*	Wilkes et al., 2017
-49.2	-44.5	-4.7	*Alexandrium tamarense*	Wilkes et al., 2017
-46.6	-44.4	-2.2	*Alexandrium tamarense*	Wilkes et al., 2017
-41.9	-42.1	0.2	*Alexandrium tamarense*	Wilkes et al., 2017
-36.6	-37.0	0.4	*Alexandrium tamarense*	Wilkes et al., 2017

Table S2. Estimating *b* from marine OM in modern-day oceans. The $\delta^{13}C$ of organic matter compiled to calculate *b* from modern marine sediments.

Location (Reference)	OM	δ_a*	SST°C†	SST°K	$\varepsilon_{b(a)}$	δ_d	ε_p	SSS‡	K_0	ε_f	$CO_{2[aq]}$	pCO_2	b
Atlantic near Portugal (*116*)	-22.3	0.50	16.2	289.2	-9.99	-10.49	12.1	37	0.0369	26.5	11.1	300	160
Gironde, France (*102*)	-20.5	0.50	15.2	288.2	-10.11	-10.61	10.1	37	0.0380	26.5	11.4	300	187
Black Sea (*99*)	-23.0	0.50	15.4	288.4	-10.09	-10.59	12.7	23	0.0404	26.5	12.1	300	167
Congo fan (*115*)	-19.8	0.50	27.2	300.2	-8.74	-9.24	10.8	37	0.0274	26.5	8.2	300	129
Amazon shelf (*98, 112*)	-18.5	0.50	28.5	301.5	-8.60	-9.10	9.6	37	0.0265	26.5	8.0	300	135
Atlantic near Brazil (*111*)	-20.0	0.50	26.5	299.5	-8.82	-9.32	10.9	37	0.0278	26.5	8.4	300	130
Arabian Sea (*101*)	-20.0	0.50	26.7	299.7	-8.80	-9.30	10.9	35	0.0279	26.5	8.4	300	131
NE Atlantic (*110*)	-19.9	0.50	13.3	286.3	-10.34	-10.84	9.2	37	0.0403	27.5	12.1	300	221
St. Lawrence, Canada (*114*)	-20.8	0.50	5.7	278.7	-11.28	-11.78	9.2	30	0.0539	26.5	16.2	300	280
Gulf of Trieste, Canada (*100*)	-21.0	0.50	17.0	290	-9.90	-10.40	10.8	37	0.0360	26.5	10.8	300	169
Santa Barbara Basin (*104*)	-21.3	0.50	14.8	287.83	-10.16	-10.66	10.9	37	0.0384	26.5	11.5	300	180
E Australian shelf (*103*)	-18.0	0.50	24.2	297.2	-9.08	-9.58	8.6	35	0.0298	26.5	8.9	300	160
Gulf of Mexico (*105, 106, 109, 113*)	-19.2	0.50	26.2	299.2	-8.85	-9.35	10.0	36	0.0282	26.5	8.5	300	139

* Averaged $\delta^{13}C$ of planktonic foraminifera *G. ruber* (*117, 118*)

† Sea surface temperature derived from seatemperature.org

‡ Sea surface salinity derived from NASA PODAAC

Table S3. Estimating *b* from phytol across an equatorial Pacific Ocean transect. The $\delta^{13}C$ of phytol (Ph) from modern marine sediments in the literature (*1*) over a 500 km transect, shown by latitude (Lat) and depth (m) used in order to calculate *b*.

Lat	m	Ph	δ_p	δ_a*	SST†	$\varepsilon_{b(a)}$	δ_d	ε_p	SSS‡	K_0	ε_f	aq	pCO_2	b
3N	78	-26.4	-22.9	0.5	27	-8.8	-9.3	14	35	0.0277	26.5	8	300	104
2N	20	-26.4	-22.9	0.5	27	-8.8	-9.3	14	35	0.0277	26.5	8	300	104
2N	44	-26.0	-22.5	0.5	27	-8.8	-9.3	14	35	0.0277	26.5	8	300	108
1N	20	-26.0	-22.5	0.5	27	-8.8	-9.3	14	35	0.0277	26.5	8	300	108
1N	44	-25.4	-21.9	0.5	27	-8.8	-9.3	13	35	0.0277	26.5	8	300	113
0	15	-26.7	-23.2	0.5	27	-8.8	-9.3	14	35	0.0277	26.5	8	300	102
0	29	-26.1	-22.6	0.5	27	-8.8	-9.3	14	35	0.0277	26.5	8	300	107
2S	25	-25.1	-21.6	0.5	27	-8.8	-9.3	13	35	0.0277	26.5	8	300	115
2S	49	-25.2	-21.7	0.5	27	-8.8	-9.3	13	35	0.0277	26.5	8	300	115

*Averaged δ13C of planktonic foraminifera *G. ruber* (*117, 118*)

†Sea surface temperature derived from seatemperature.org

‡Sea surface salinity derived from NASA PODAAC

Code S1. Python code used for Monte Carlo simulations to calculate uncertainty for P_{CO_2} estimations by considering every parameter involved in the equations.

Data S1. All data used to reconstruct P_{CO_2} from the $\delta^{13}C_{phytane}$.